JOURNAL OF MATERIALS SCIENCE 32 (1997) 5505–5511

Deformation and fracture of styrene–acrylonitril copolymer – rubber blends

Microscopy studies of deformation zones

A. C. STEENBRINK‡, H. JANIK*, R. J. GAYMANS
Department of Chemical Engineering, University of Twente, The Netherlands
** Chemical Faculty, Technical University of Gdansk, 80952 Gdansk, Poland*

A styrene–acrylonitril copolymer (SAN) was toughened by SAN-grafted polybutadiene core-shell rubber particles. Notched tensile specimens were fractured with a tensile speed ranging from 10^{-4} to 10 m s^{-1}. The deformation processes close to the fracture surface were studied by means of transmission electron microscopy. A marked difference in the structure of the deformation zone was observed between low speed (10^{-3} m s^{-1}) and high speed (≥ 1 m s^{-1}) deformed samples. At low tensile speed the structure of the deformation zone correlated closely with fracture mechanics theory. When the tensile speed was increased the deformation zone had a layered structure. In the zone 400–1.5 μm below the fracture surface the deformation structure was similar to that at low speed. In the layer 1.5–0.5 μm from the fracture surface the rubber particles were strongly deformed, but no cavities or crazes could be observed. Directly next to the fracture surface the high speed deformation zone showed a small layer (0.5 μm) where all the deformation had vanished. It is suggested that due to high strain-rate plasticity at the crack tip a temperature rise occurs which is high enough to cause complete relaxation of the deformation in this layer. Therefore, locally the glass transition temperature of the matrix material was reached. The interaction between thermal effects and deformation processes at the crack tip is discussed.

1. Introduction

The enhancement of fracture toughness by the incorporation of rubber particles in a brittle amorphous polymer matrix is highly dependent on the morphology of the material. The toughening micromechanism is considered to be shear deformation promoted by cavitation of rubber particles [1–4]. Matrix crazing is regarded both as a toughening and a damaging mechanism. The significance of these mechanisms may vary with material parameters, in particular with rubber particle size, matrix molecular weight and matrix entanglement density and with test conditions like temperature, strain rate and stress state.

In addition to the commonly observed toughening of rubber-modified polymers an enhanced toughening is observed in several rubber modified polymers at very high deformation speeds [5–7].

Boode *et al.* [8] showed that at high speed fracture the deformed microstructure of an acrylonitril-butadiene-styrene (ABS) Izod specimen was different from finite element predictions. According to the numerical model the amount of deformation and the alignment with the fracture direction increases when one approaches the fracture surface. Using transmission electron microscopy (TEM) it was shown that directly next to the fracture surface there was a small layer where the deformation was much less than at a larger distance from the fracture surface (Fig. 1(a–d)). We believe that this can only be explained by the notion of a temperature rise at the crack tip causing relaxation of the deformation in a small zone around the crack tip.

In particular in nylon–rubber blends a temperature effect during crack propagation was made plausible [9]. From TEM micrographs, a layer with undeformed or relaxed particles was observed next to the fracture surface of samples broken at very high speeds (1–10 m s^{-1}). Polarized light microscopy was used to reveal changes in the birefringence with the distance from the fracture surface. At a low deformation speed (10^{-3} m s^{-1}) an increasing degree of orientation was found approaching the fracture surface. At high deformation speeds the degree of orientation also increased, but an unoriented layer was observed directly next to the fracture surface. TEM selected area electron diffraction was used to analyse the crystal structure of the nylon. The annealed nylon blend was in the α-structure. Close to the fracture surface, however, the material had the γ-structure which is typical for

‡ Presently at: Department of Mechanical Engineering, Delft University of Technology, The Netherlands.

0022–2461

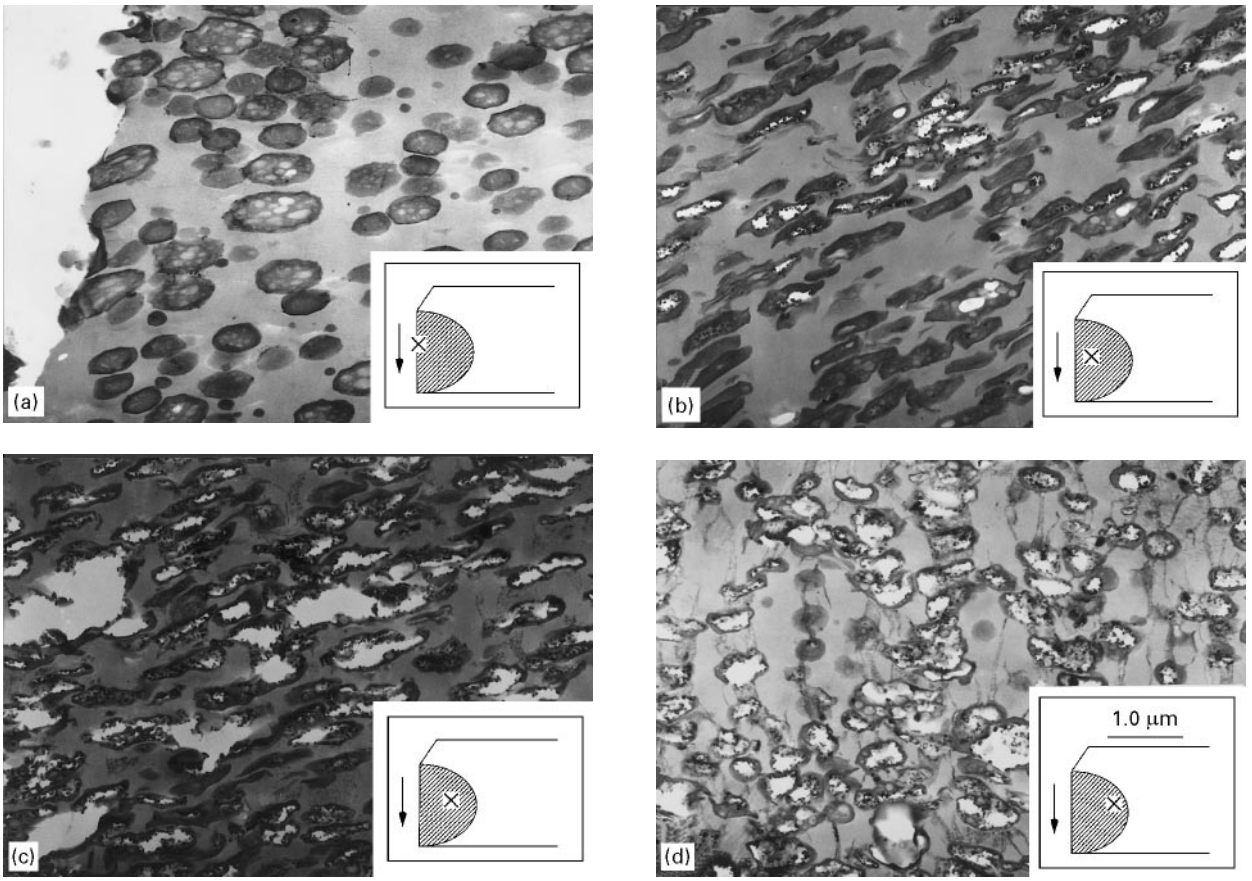

Figure 1 TEM micrographs at different locations in the deformation zone of an ABS notched fractured Izod specimen. The sections were taken perpendicular to the fracture direction. The arrow indicates the fracture direction. The dashed area represents the stress-whitening zone. (a) taken directly at the fracture surface (left edge), (b) 50 μm from the fracture surface, (c) 100 μm from the fracture surface, (d) 250 μm from the fracture surface. The pictures were kindly supplied by J. W. Boode *et al.* [8].

quenched material. So it was concluded by Janik *et al.* [9] that the material had melted (and cooled rapidly) during the fracture process.

In this paper we report the results of a TEM study on the structure of the deformation zone next to the fracture surface in a blend of styrene–acrylonitril (SAN) with a SAN-grafted polybutadiene (PB) core-shell rubber at various deformation speeds.

2. Experimental procedure

An extrusion blend of a styrene–acrylonitril copolymer (TYRIL 790, supplied by the Dow Chemical Company) and a SAN-grafted polybutadiene (GRC 310, supplied by Dow) was prepared in a Berstorff ZE 25 corotating twin screw extruder. The PB rubber content was 30 vol %. The particle size was in the range of 0.1 μm. Injection moulded bars ($72 \times 10 \times 4$ mm) with a sawed notch were used for tensile test on a Schenk VHS servo-hydraulic tensile machine. The specimen length between the clamps was 42 mm.

The structure of the deformation zone was studied by means of transmission electron microscopy (TEM). Microscopy samples were taken from notched specimens broken at clamp speeds of 10^{-3}, 10^{-2}, 1 and 10 m s^{-1}. The average strain rate in the sample varied from 0.024 s^{-1} at 10^{-3} m s^{-1} to 240 s^{-1} at 10 m s^{-1}.

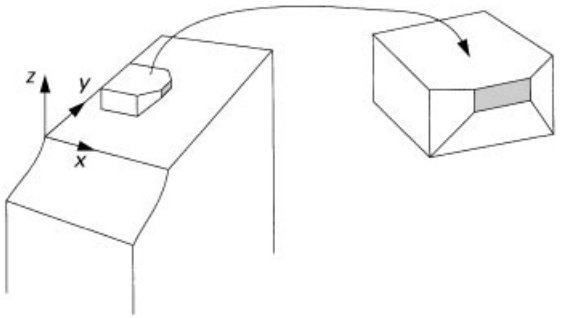

Figure 2 Microscopy sample taken from a notched fractured tensile specimen. The fracture plane is the x–y plane. The fracture and tensile direction are the y- and z-direction, respectively. The plane of TEM-investigation is the y-z plane (shaded).

The plane of investigation was spanned by a vector in the fracture direction and a vector in the tensile direction (the y–z plane in Fig. 2). The samples were taken from the middle of the fracture plane. We studied the deformation structure both directly next to the fracture surface as well as deeper inside the specimen, but always well inside the stress-whitening zone. Cutting has been done with a CryoNova microtome at room temperature. The direction of cutting was in the fracture direction. The samples were prepared in three stages. Between each preparation step the samples were stained in a 2% aqueous solution of OsO_4 at

40 °C for at least 72 h. First, the sample was trimmed with a glass knife to a wedge shape in order to reduce the dimensions of the cutting area. Then ultrathin slices were cut with a wet diamond knife to remove possible deformation caused by trimming. Finally, ultra-thin sectioning was performed with a wet diamond knife and the sections were collected on a 400 mesh microscope grid.

The slices were studied on a Jeol-200CX TEM operating at 200 kV with a very low dose of the electron beam in order to prevent destruction of the sample.

3. Results

3.1. Mechanical properties

The fracture toughness was measured as a function of deformation speed [7]. We studied notched tensile specimen on a servo-hydraulic tensile machine. The speed of the clamps was in the range of 10^{-4}–10 m s^{-1}. The total energy dissipation was calculated from the force–time signals and the results are shown in Fig. 3. Increasing the deformation speed from 10^{-3} to 1 m s^{-1} had little affect on the total energy dissipation. The amount of stress-whitening next to the fracture surface decreased (Fig. 3). When the deformation speed was increased to 10 m s^{-1}, the energy dissipation increased and also the amount of stress whitening increased. This might indicate that in the high speed region another mechanism of energy dissipation becomes operative.

3.2. Microscopy studies of morphology and deformation zones

3.2.1. Morphology of the undeformed material

The undeformed material was studied in order to determine the morphology of the blend. We also checked if the preparation method for the electron microscopy studies caused any kind of deformation. The structure of the undeformed material is shown in Fig. 4. The average particle size was 0.1 μm. The particle size distribution was very narrow. There was also a small number of larger particles, with a size in the range of 0.3–0.5 μm. The small particles with a size of about 0.1 μm did not contain any glassy subinclusions. In the larger particles minor inclusions of matrix material could occasionally be observed.

3.2.2. Deformation zones

The structure of the deformation zone directly at the fracture surface was examined as a function of tensile speed. Transmission electron micrographs of sections taken directly at the fracture surface are shown in Fig. 5(a–d). Micrographs of sections taken at larger distances from the fracture surface will be presented at the appropriate points in this paper.

3.2.3. Material deformed at low speed (*LS*, 10^{-3} m s^{-1})

The deformation zone next to the fracture surface is shown in Fig. 5a. The rubber particles were cavitated and strongly elongated indicating large plastic shear deformation. The aspect ratio of the rubber particles (which can be used as an approximate measure for the local principal strain) was of the order of 5. Directly next to the fracture surface the particles were almost completely aligned with the fracture direction which suggests a very high degree of orientation. Thick crazes were present between practically all the particles (Fig. 6). A decreasing elongation and alignment to the fracture direction was observed as we moved away from the fracture surface. These observations are in qualitative agreement with the deformation and stress distribution around a crack tip, which can be approximately calculated using fracture mechanics [10, 11].

Further away from the fracture surface (100–300 μm) the deformation was not homogeneous. The deformation processes (crazing, shear and cavitation) were concentrated in bands perpendicular to the tensile direction (Fig. 7). Between these bands there was apparently few deformation, i.e., the rubber particles were round and not cavitated and also no crazes in the matrix were observed. It has been previously observed that rubber particle cavitation encourages cavitation of neighbouring particles [12–14].

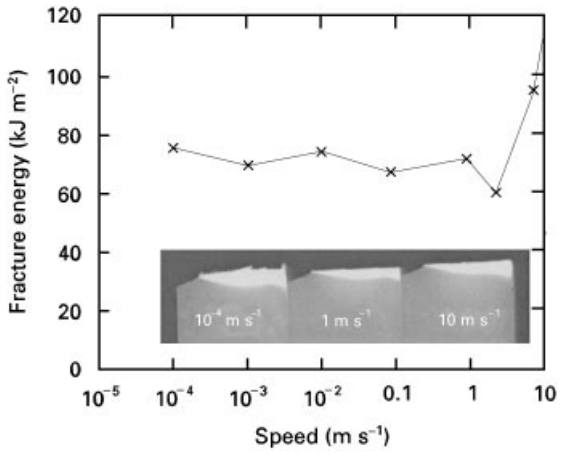

Figure 3 Energy dissipation as a function of deformation speed for ABS with 30 vol % PB. The amount of stress-whitening is indicated for various tensile speeds.

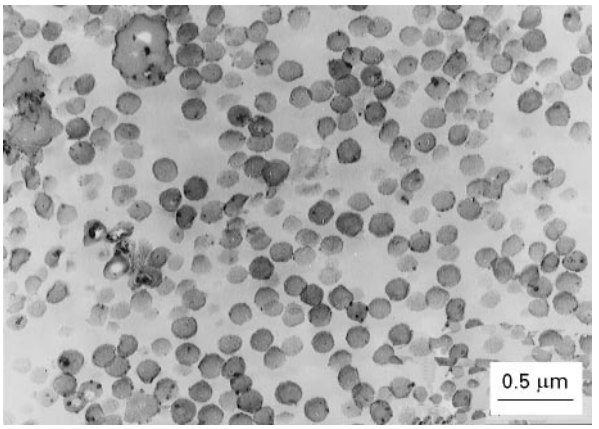

Figure 4 TEM picture of the internal morphology of an undeformed injection moulded bar of ABS with 30 vol % PB.

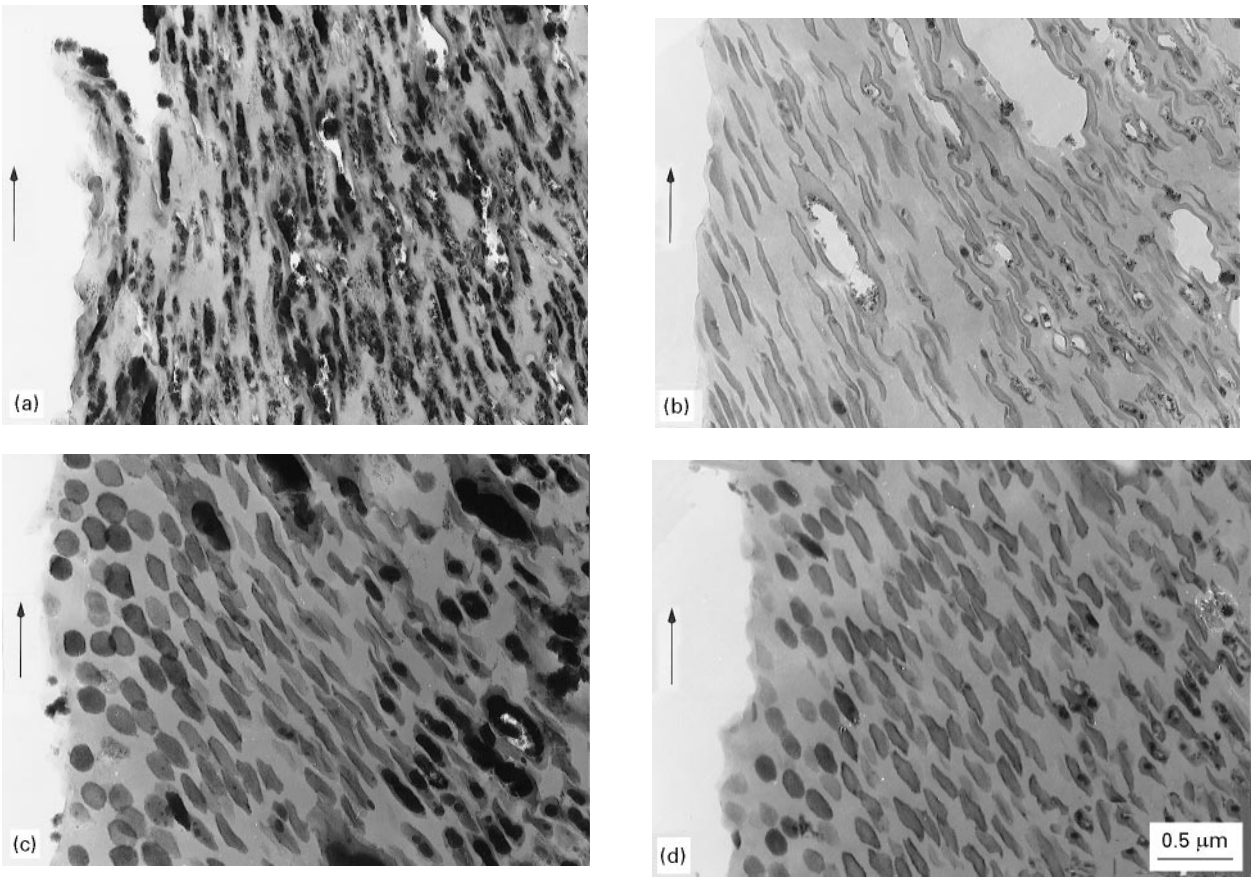

Figure 5 TEM micrographs in the deformation zone perpendicular to the fracture surface of an ABS notched tensile specimen. The arrow indicates the fracture direction. The samples were fractured at different tensile speeds. (a) 10^{-3} m s^{-1}, (b) 10^{-2} m s^{-1}, (c) 1 m s^{-1}, (d) 10 m s^{-1}. In the high speed deformed samples (c and d) three zones can be distinguished: (i) a "relaxed" layer with round solid particles, (ii) a layer with elongated rubber particles without crazes, (iii) below matrix crazing and shear as well as particle cavitation can be observed.

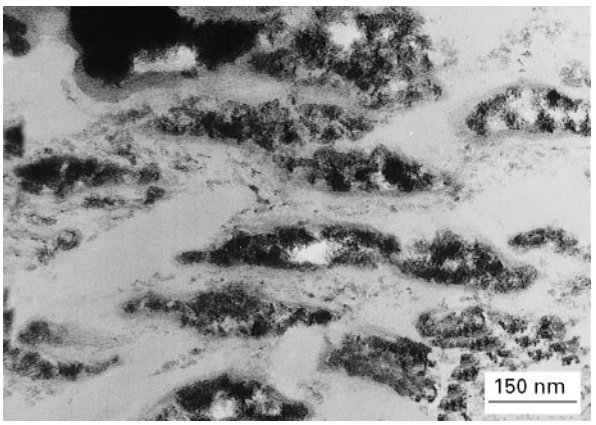

Figure 6 Detail of the deformation zone in Fig. 5a. The deformation speed is 10^{-3} m s^{-1}. The particles are cavitated and strongly elongated. In between there are thick crazes.

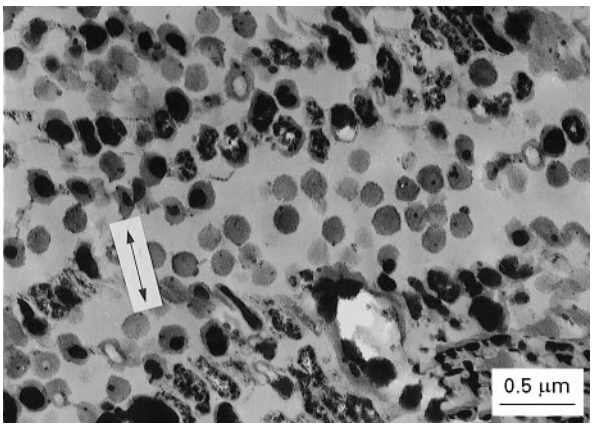

Figure 7 Deformation zone at a distance of 160 μm from the fracture surface. The deformation speed is 10^{-3} m s^{-1}. Concentrated bands of deformation normal to the tensile direction with apparently few deformation in between. The (local) tensile direction is indicated with the arrow.

3.2.4. Material deformed at medium speed (*MS, 10^{-2} m s^{-1}*)

Far away from the fracture surface the deformation field was similar to that of the low speed samples although the elongation and angle of alignment were smaller (Fig. 5b). Nevertheless it was clear that matrix crazing and shear yield as well as rubber particle cavitation had occurred. Like at low speed (LS) the particles showed an increasing elongation and alignment when we approached the fracture surface. In a layer next to the fracture surface (0–1 μm) the rubber particles were elongated and aligned with the fracture direction but no crazes or cavities could be observed.

3.2.5. Material deformed at high speed (*HS, 1 m s^{-1}*)

At high speed (1 m s^{-1}, Fig. 5c) we could distinguish three zones. Far away from the fracture surface the

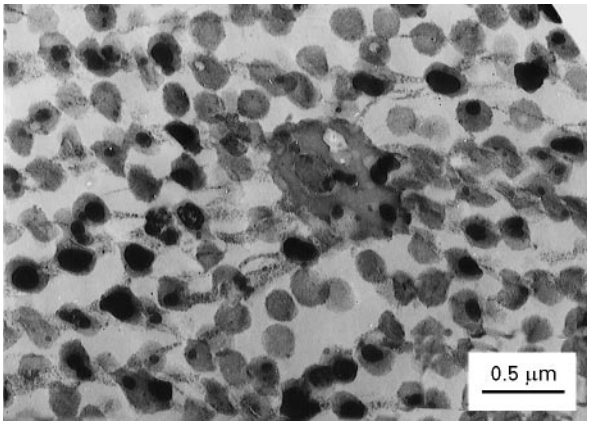

Figure 8 Deformation zone at a distance of 90 μm from the fracture surface. The deformation speed is 1 m s^{-1}. Crazes are initiated from both cavitated (heavy black) and non-cavitated rubber particles.

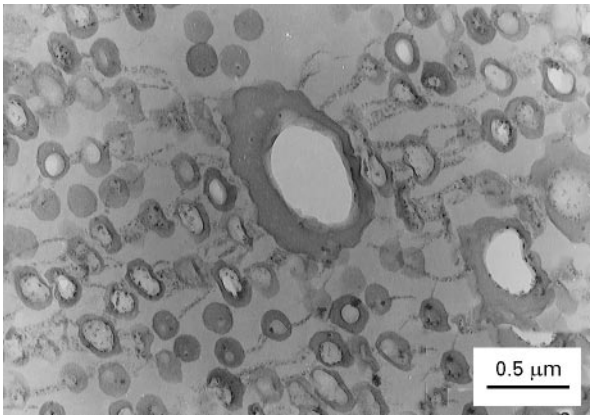

Figure 10 Deformation zone at a distance of 50 μm from the fracture surface. The deformation speed is 10 m s^{-1}. Thick crazes and large cavities are present in bands.

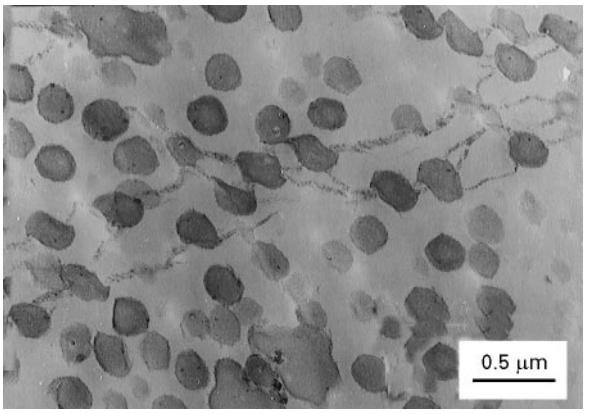

Figure 9 Deformation zone at a distance of 300–400 μm from the fracture surface. The deformation speed is 1 m s^{-1}. Thin crazes are initiated from solid, non-cavitated rubber particles.

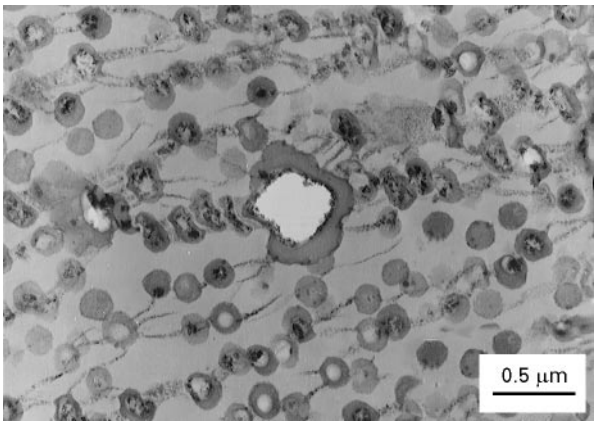

Figure 11 Deformation zone at a distance of 100 μm from the fracture surface. The deformation speed is 10 m s^{-1}.

deformation field was similar to that at medium speed. Again matrix crazing and shear yield as well as rubber cavitation had occurred. Closer to the fracture surface (0.5–1.5 μm) there was a zone where the rubber particles had elongated but they were not cavitated. Crazing of the matrix was not observed in this layer. Directly at the fracture surface (0–0.5 μm) the rubber particles were round which suggests that all the deformation that occurred prior to fracture disappeared.

At a distance of 90 μm from the fracture surface we saw that crazing was initiated from both cavitated and non-cavitated rubber particles (Fig. 8). At 400 μm we saw thin crazes running from solid, non-cavitated rubber particles (Fig. 9). At this moment we are uncertain as to if the particles were uncavitated at the moment of craze initiation. It might be possible that the cavities close during elastic unloading. This could be established by using a real-time small angle X-ray scattering (RTSAXS) technique.

3.2.6. Material deformed at very high speed (*VHS, 10 m s^{-1}*)

At very high speed (10 m s^{-1}, Fig. 5d) we again distinguished three zones, very similar to the structure of the HS sample. The first layer with apparently undeformed particles had a thickness of 0.5 μm, which was the same as at HS. The second zone without crazes had a thickness of 2.5 μm, which was more than at HS.

At a distance of 50 μm from the fracture surface large cavities and thick crazes were visible (Fig. 10). The deformation was inhomogeneous. It seems that cavities preferentially grow in bands. At 100 μm the cavities and crazes were smaller (Fig. 11). At this distance crazes are always initiated from cavitated rubber particles.

4. Discussion

The structure of the deformation zone at higher deformation speeds (MS, HS and VHS) was quite different from that at low speed (LS). We have also observed an enhanced energy dissipation at high deformation rates [7]. Furthermore, when the tensile speed was increased from 1 to 10 m s^{-1} the amount of stress-whitening increased unexpectedly. These results indicate that in the high speed regime an additional fracture process becomes operative.

The transmission electron micrographs show clear evidence of relaxation of the deformation. We think this "relaxed" deformation layer is the result of a local temperature rise due to adiabatic heat production at

the crack tip. The first indication for strong thermal effects during fracture occurred at 10^{-2} m s^{-1} (MS). A small layer without crazes or cavities was found directly next to the fracture surface. As the tensile speed increased the thermal effects became stronger. At 1 m s^{-1} and higher complete relaxation in a small layer at the fracture surface took place. This relaxation layer has been observed also in polymer-rubber blends with semi-crystalline matrices like polypropylene and nylon [6, 12]. In those materials the material softens instantaneously at the melting temperature T_m. Just above T_m complete relaxation of the deformation takes place. The material properties of toughened amorphous SAN are affected in a relatively wide range around the glass transition temperature T_g. This is in fact illustrated by the deformation zone at 10^{-2} m s^{-1} (MS). At this speed the crack tip temperature may not reach T_g but partial relaxation of the deformation has taken place. It is suggested that relaxation of the deformation at HS and VHS was possible at a temperature close to the glass transition temperature.

The coupled thermo-mechanical behaviour of polymers has been recognized for a long time. Early theories on the plasticity of polymers attributed the plastic deformability to the temperature rise accompanying the deformation. Also the necking process was thought to be caused by thermal softening. Although these theories have proven to be inadequate to describe yield and necking, it is generally accepted that high strain rate plasticity is usually accompanied by a significant temperature rise. The thermal blunting concept has been used to explain the variation of fracture toughness with strain rate for glassy polymers by Williams and Hodgkinson [15].

We have recently carried out online temperature measurements during deformation of notched and unnotched specimen of ABS using an infrared thermal imaging system. In this case we also observed significant thermal effects during plastic deformation and fracture. A temperature rise up to the glass transition temperature was measured [16, 17].

It also remains to be established what the interaction is between crazing and cavitation. Both mechanisms are likely to be driven by the hydrostatic component of the stress. When a rubber particle cavitates, the deformation field around the particle is changed drastically, which could be accompanied by the initiation or growth of crazes. Usually we observed crazes only at cavitated rubber particles. At 1 m s^{-1} at 400 μm from the fracture surface however, we observed craze initiation from solid, non-cavitated rubber particles. It has also been observed that particle cavitation occurred on the path of crazes that were initiated from larger particles [18]. In that study, however, the rubber particles contained many subinclusions which makes the results difficult to compare. In general the contribution to the dilatation of both mechanisms will be highly dependent on the constitution of both phases in the blend and on the test conditions. Internal cavitation of the rubber particles seems to be dominated by two factors: rubber modulus and surface energy [13, 18, 19]. Cavitation will be favoured in larger particles with a low elastic modulus.

5. Conclusions

The morphology of a SAN-copolymer with a SAN-grafted PB core-shell rubber blend has been studied with TEM for undeformed as well as notched fractured samples. The deformation processes that have been observed are internal cavitation of the rubber particles, large shear deformation and crazing of the SAN matrix.

The deformation zone in low speed deformed samples (10^{-3} m s^{-1}) showed an increasing elongation and alignment when we approached the fracture surface. Further away from the fracture surface the deformation processes were inhomogeneously distributed in bands perpendicular to the tensile direction.

At medium speed (10^{-2} m s^{-1}) in a layer next to the fracture surface (0–2 μm) the rubber particles were elongated and aligned, but no crazes or cavities could be observed. Outside this layer the common deformation processes have been observed.

In high speed deformed samples (1 m s^{-1}) we could distinguish three layers. First there was a "relaxed" layer with round solid particles directly next to the fracture surface (0–0.5 μm). From 0.5 to 1.5 μm the particles were elongated without cavitation and craze formation in the matrix. Further away matrix crazing and shear as well as particle cavitation could be observed.

The same structure was observed in VHS samples (10 m s^{-1}) although the second layer with non-cavitated shear deformed particles was thicker (2.5 μm). The appearance of a layer where the deformation has relaxed was explained by a temperature rise during crack propagation.

The isolation of a direct relationship between the temperature rise and the fracture toughness enhancement at very high deformation speed needs further research. Also the sequence and interaction of matrix crazing and rubber particle cavitation should be investigated by RTSAXS experiments.

Acknowledgement

This work was sponsored by the Netherlands Technology Foundation (STW). The authors wish to thank J. W. Boode for supplying the pictures used in Fig. 1.

References

1. C. B. BUCKNALL, "Toughened Plastics", (Applied Science, London, 1977).
2. F. RAMSTEINER, *Polymer* **20** (1979) 839.
3. A. M. DONALD and E. J. KRAMER, *J. Mater. Sci.* **17** (1982) 1765.
4. B. Y. NI, J. C. M. LI and V. K. BERRY, *Polymer* **32** (1991) 2766.
5. K. DIJKSTRA, J. TER LAAK and R. J. GAYMANS, *ibid.* **35** (1994) 315.
6. A. VAN DER WAL and R. J. GAYMANS, in Proceedings of the Materials Institute Conference; Deformation Yield and Fracture of Polymers, Cambridge, April 1994, Preprints poster 60.
7. A. C. STEENBRINK and R. J. GAYMANS, *ibid.* Preprints poster 117.
8. J. W. BOODE, A. E. H. GAALMAN, A. J. PIJPERS and R. J. M. BORGGREVE, in Proceedings of the Prague Macromol. Meetings, Prague, 1990, poster.

9. H. JANIK, R. J. GAYMANS and K. DIJKSTRA, *Polymer* **36** (1995) 4203.
10. D. BROEK, "Elementary Engineering Fracture Mechanics", (Nijhoff, Dordrecht, 1986).
11. J. G. WILLIAMS, "Fracture Mechanics of Polymers", (Ellis Horwood, Chichester, 1984).
12. K. DIJKSTRA and R. J. GAYMANS, *J. Mater. Sci.* **29** (1994) 3231.
13. A. LAZZERI and C. B. BUCKNALL, *ibid.* **28** (1993) 6799.
14. C. CHENG, A. HILTNER, E. BAER, P. R. SOSKEY and S. G. MYLONAKIS, *ibid.* **30** (1995) 587.
15. J. G. WILLIAMS and J. M. HODGKINSON, *Proc. Roy. Soc. Lond.* **A 375** (1981) 231.
16. A. C. STEENBRINK, R. J. GAYMANS, and E. van der GIESSEN, Proceedings of European Symposium on Polymer Blends, Maastricht, May 12–15, 1966, p. 222.
17. A. C. STEENBRINK, Ph.D. thesis, Delft University of Technology, 1997.
18. Y. OKAMOTO, H. MIYAGI and S. MITSUI, *Macromolecules* **26** (1993) 6547.
19. A. N. GENT and D. A. TOMPKINS, *J. Polym. Sci. Part A-2* **7** (1969) 1483.

Received 20 November 1995
and accepted 21 March 1997